

## Hierarchical microstructure of explosive joints: Example of titanium to steel cladding

J. Song<sup>a</sup>, A. Kostka<sup>a,\*</sup>, M. Veehmayer<sup>b</sup>, D. Raabe<sup>a</sup>

<sup>a</sup> Max-Planck Institut für Eisenforschung GmbH, Max-Planck Str. 1, 40237 Düsseldorf, Germany

<sup>b</sup> Dynamic Materials Corporation GmbH, Dr. Hermann-Fleck-Allee 8, 57299 Burbach, Germany

### ARTICLE INFO

#### Article history:

Received 26 August 2010

Received in revised form

29 November 2010

Accepted 30 November 2010

Available online 8 December 2010

#### Keywords:

Explosive welding

Electron microscopy

Steel

Titanium

Interfaces

### ABSTRACT

The microstructure of explosive cladding joints formed among parallel Ti and steel plates was examined by electron microscopy. The bonding interface and the bulk materials around it form pronounced hierarchical microstructures. This hierarchy is characterized by the following features: at the mesoscopic scale of the hierarchy a wavy course of the interface characterizes the interface zone. This microstructure level is formed by heavy plastic shear waves (wavelength  $\approx 0.5$  mm) which expand within the two metal plates during the explosion parallel to the bonding interface. At the micro-scale range, intermetallic inclusions (size  $\approx 100$ – $200$   $\mu\text{m}$ ) are formed just behind the wave crests on the steel side as a result of partial melting. Electron diffraction revealed FeTi and metastable  $\text{Fe}_{9.64}\text{Ti}_{0.36}$ . Most of the observed phases do not appear in the equilibrium Fe–Ti phase diagram. These intermetallic inclusions are often accompanied by micro-cracks of similar dimension. At the smallest hierarchy level we observe a reaction layer of about 100–300 nm thickness consisting of nano-sized grains formed along the entire bonding interface. Within that complex hierarchical micro- and nanostructure, the mesoscopic regime, more precisely the type and brittleness of the intermetallic zones, seems to play the dominant role for the mechanical behavior of the entire compound.

© 2010 Elsevier B.V. All rights reserved.

### 1. Introduction

The challenge of developing materials for advanced structural applications is gradually shifting from the optimization of novel bulk materials to the synthesis of compounds that contain metallurgical joints.

This means that the design of modern metallic compounds must be built on a detailed microstructure-oriented understanding and property optimization of the underlying interfaces at the joints between dissimilar bulk metals.

This task is particularly challenging for joints among bulk metals that form brittle intermetallic phases when conventionally welded such as steel and aluminum or steel and titanium.

This work is about the latter combination. Titanium has excellent corrosion resistance and strength-to-weight ratio. Its alloys are used in multiple energy and chemical industry infrastructure and periphery applications [1]. When such devices require plates of multiple mm thickness or very high strength, Ti alone is often insufficient. Hence an increasing demand exists for combining the functional properties of Ti with structural support materials by plate joining it with steels.

Conventional welding of Ti and steel is very challenging though due to (i) the high reactivity of Ti with oxygen and nitrogen at high temperatures [2,3] and (ii) the formation of brittle intermetallic compounds, such as FeTi and  $\text{Fe}_2\text{Ti}$ , at the joint interface [4]. Moreover, significant differences in their physical properties like heat transfer and thermal expansion coefficient could introduce large residual stresses in the interface region.

Explosion welding is an efficient alternative to conventional joining in this case [5–7]. It works by accelerating the top plate (here: Ti) to a very high velocity towards the substrate plate (here: steel) through the ignition of an explosive coating on its surface. Before the explosion the two parallel plates are separated by several mm using small columns. During the process, the plates are heavily deformed close to the newly formed interface and the surfaces are brought into close contact, sufficient to create a metallurgical bond. The high rate of the process minimizes the interdiffusion length and hence reduces the formation of brittle intermetallic components at the bonding interface.

Three external process parameters mainly control the jet expansion between the plates and the collision, namely, the explosive mass, collision angle and stand-off distance, Fig. 1. At the mm-scale the joint shock wave and collision processes produce a characteristic wavy interface among the two plates.

Although the jet dynamics and the transient fluid-like behavior of the abutting materials under high pressure in the collision zone

\* Corresponding author. Tel.: +49 211 6792 989; fax: +49 211 6792 333.  
E-mail address: [a.kostka@mpie.de](mailto:a.kostka@mpie.de) (A. Kostka).

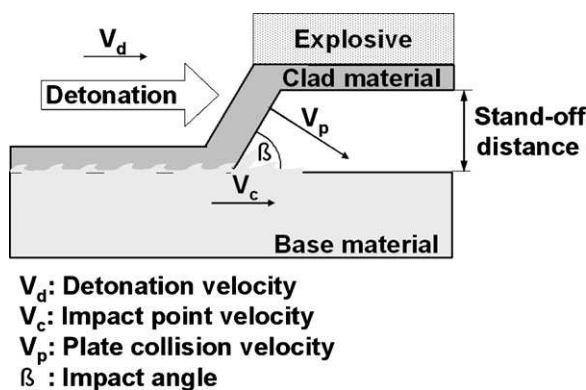


Fig. 1. Processing parameters during an explosive cladding process.

have been studied from an engineering and gas dynamical perspective [8–10] it becomes increasingly apparent that as a rule not the details of the wave pattern, but the resulting complex microstructures determine the mechanical properties of the clad products [8,9].

It is, therefore, the aim of this investigation to characterize and better understand the graded microstructures at the bonding zone and their metallurgical formation processes with regard to the mechanical behavior. Particular attention is placed on two aspects: The first one is the fact that the interfacial microstructures reveal a pronounced hierarchical pattern with characteristic defects arrangements at different positions relative to the bonding interface. The second one is the aim to identify which of these microstructural ingredients is essential for damage initiation in these materials.

Cladding systems that have been addressed so far are Al/Al [10], Al/Cu [11], Al/steel [12], Cu/Cu–2Be [13], Mo/Cu [14], Ti/stainless steel [5], Ti/Ti [15], high Mn steel/low C steel [16], and Ti/low C steel [17]. In these works techniques such as optical microscopy, scanning electron microscopy (SEM), and microhardness testing were used to characterize the microstructure. They mostly focused on the manufacturing procedures, explosive conditions, and bonding strength. Recently, studies of morphology and structure at the bonding interfaces were conducted using also transmission electron microscopy (TEM) [18]. No investigation, however, revealed the entire microstructure hierarchy at the bonding interfaces owing to the limited volume accessible to TEM, i.e. a comprehensive analysis of the characteristic features of the microstructures at different scales of explosive clad components does not yet exist. In order to develop explosive clads with good mechanical properties (high shear and normal resistance; high damage tolerance; ductile failure), it is essential to understand the metallurgical mechanism of the bonding and the underlying microstructures at different scales.

In this study, we characterize and discuss the hierarchy of the microstructure and phase formation of a Ti/steel clad interface. The investigation of the reaction products formed at the cladding interface was carried out using electron diffraction techniques and chemical analysis (EDX). We observe that the microstructure has a pronounced hierarchy which is characterized by specific defect and phase composition and topologies at various length scales. The interplay of the different hierarchical levels in the sample under load determines the mechanical properties of the joint.

## 2. Experimental procedures

A commercial purity Ti plate (average grain size of  $5.2 \mu\text{m}$ ) and a steel sheet (average grain size of  $10.2 \mu\text{m}$ ) were joined by explosive cladding, Table 1. Specimens for microstructure analysis were extracted from the central part of the joint in a plane parallel to

**Table 1**  
Chemical composition of joined components (at.%).

	Al	C	Cu	Mn	P	Fe	Cr	Ni	Si	Ti
Steel	0.04	0.18	0.02	0.98	0.01	Bal.	0.03	0.03	0.3	–
Ti	0.003	0.01	–	–	–	0.02	–	–	–	Bal.

the detonation direction and normal to the plane of the cladding interface using spark erosion, Fig. 2.

Specimens for SEM were prepared via grinding and polishing. Microstructure examination was carried out using a Jeol JSM-6500F SEM operated at 15 kV. TEM analysis was conducted using a Jeol JEM-2200FS instrument operated at 200 kV. Samples for TEM analysis were prepared using a Jeol JEM-9320 focused ion beam (FIB) system operated at 30 kV. Since chemical compositions determined by EDX did not follow the Fe–Ti phase diagram, phase identification (not shown in detail here) of all components of the interface was conducted via systematic analysis of electron diffraction patterns acquired in TEM.

The specimens for standard flat tensile and bending testing were extracted as shown in Fig. 2. A three-point bending test was employed to evaluate the mechanical properties of the joints. Specimens with a size of  $3 \text{ mm} \times 3 \text{ mm} \times 25 \text{ mm}$  was extracted from the joints in the plane perpendicular to the detonation direction. During bending the samples were oriented in such a way that Ti was under compressive and the steel substrate under tensile load.

## 3. Results

The interface region formed by explosive cladding has a complex and hierarchical structure including a variety of lattice defects and non-equilibrium phases. The microstructural details of the different hierarchical unit are presented below.

### 3.1. Macroscopic overview

Visual and light optical inspection of the joint reveals a structure without visible cracks, pores, or separation of the joined components. Fig. 3 shows the formation of a typical wavy interface. The deformation of the cladding Ti plate was not homogenous: the cross-section reveals that the Ti is characterized by equiaxed grains. Towards the interface the density of deformation twins increases strongly. Moreover, due to the relatively low heat conductivity and high adiabatic shear sensitivity of Ti at high strain rates [19],

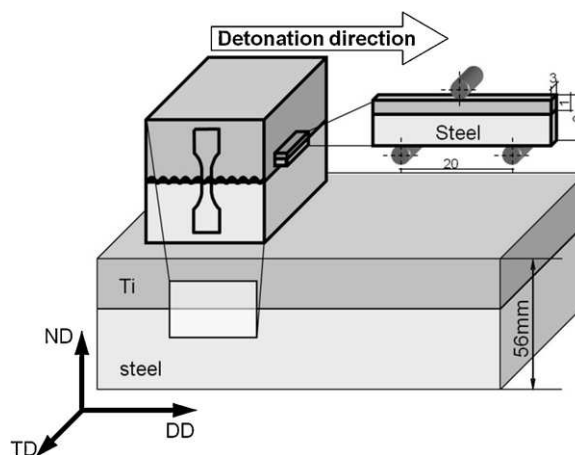
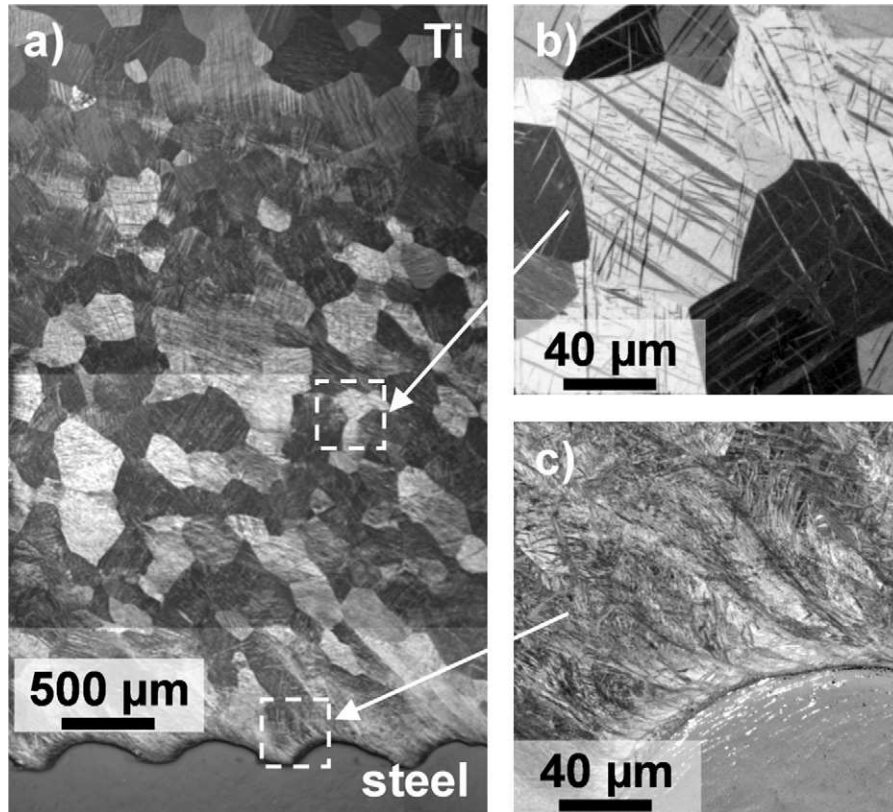


Fig. 2. Illustration of the tensile and bending specimen used to examine the mechanical properties of the joint. The steel/Ti interface of bending samples is located in such a way that Ti was under compressive and the steel substrate under tensile load; ND, normal direction; TD, transversal direction; DD, detonation direction.



**Fig. 3.** Optical micrograph showing the structure of the Ti clad plate and the wavy interface formed between the joined components (a), towards the interface line the deformation twins density increases (b) and adiabatic shear bands (ASBs) occur in the vicinity of the bonding interface (c).

adiabatic shear bands (ASBs) occur in the vicinity of the bonding interface. They appear inclined at about 45° to the detonation direction and at up to 0.5 mm distance from the interface line. The deformation zone in the steel substrate plate is characterized by elongated grains adjacent to the bonding zone. This zone is limited to an area within about 0.5 mm from the interface.

3.2. Mesoscopic and microscopic scale

The mesoscopic scale of the hierarchical structure reveals that the waves have a period of 600 μm at a relatively constant amplitude of about 150 μm, Fig. 4a. The wave formation is a consequence of the collision impact angle that is created by the explosion and

jet parameters, the stand-off distance between the sheets, and the associated plastic deformation of base materials. The mechanical energy released during impact leads to a rapid pressure boost, intense plastic deformation in the interface region, friction, and shear of the two materials. This leads to partial melting of the wave crest regions and to the formation of intermetallic inclusions, Fig. 4b. Rapid solidification and further cooling of the dissimilar partners causes micro-cracks within some of the brittle intermetallic phases, Figs. 4b and 5, which were not visible at the light optical scale.

A closer analysis of the molten region (Fig. 5) reveals a non-uniform swirl like contrast inside the inclusion indicating phase intermixing and strong gradients in the chemical composition.

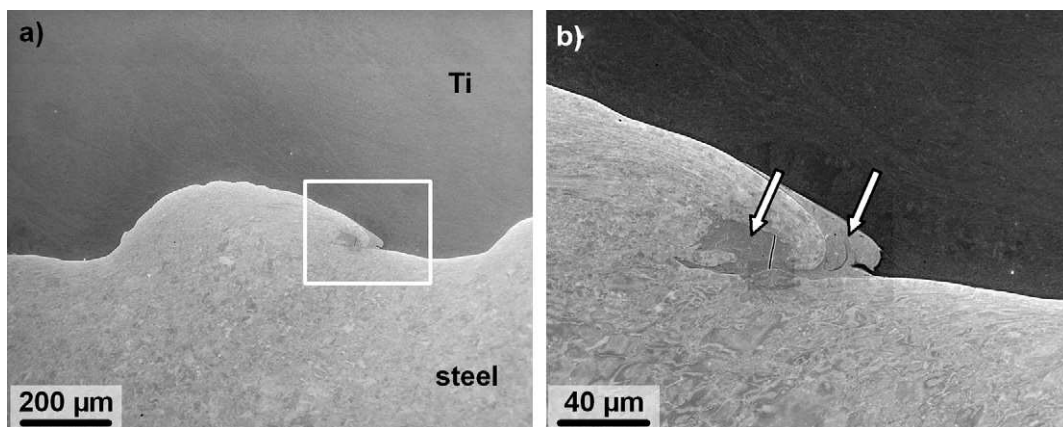


**Fig. 4.** SEM (BSE) micrograph of the interface region showing formation of intermetallic inclusions at the wave crest regions. (a) These intermetallic inclusions (see arrows) are mainly present in the steel and they are very often accompanied by micro-cracks perpendicular to the interface line (b).

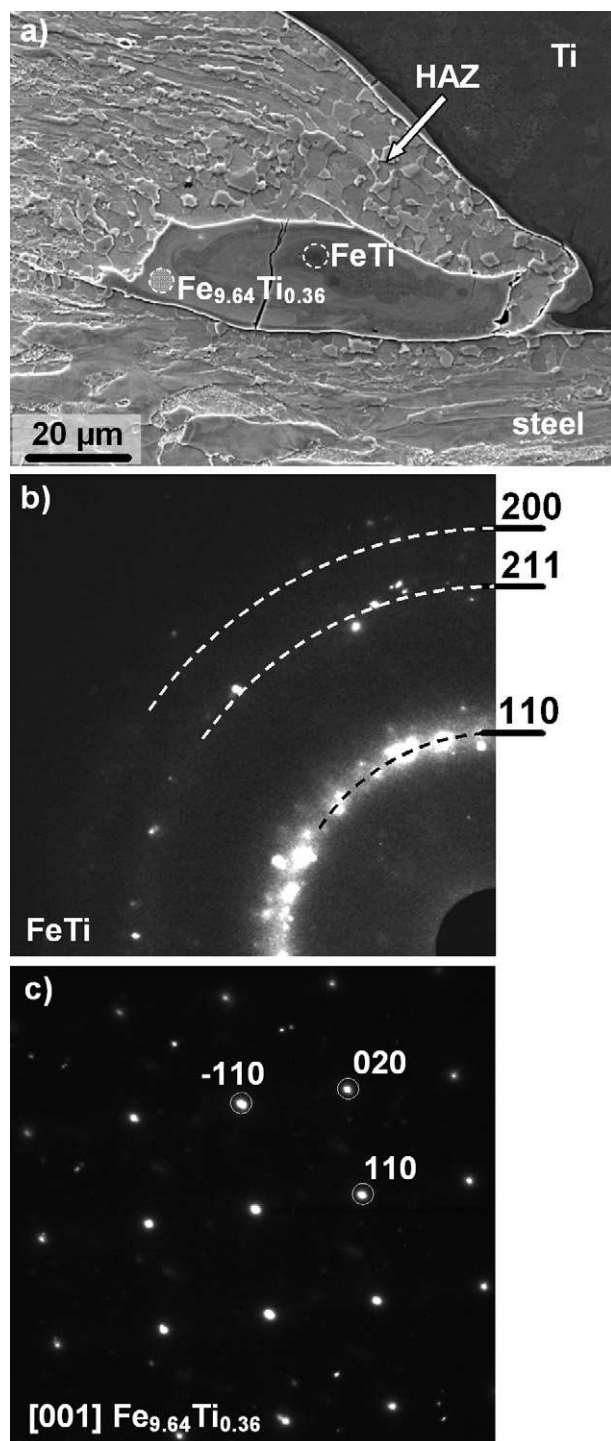


**Fig. 5.** SEM (back scattered electron (BSE) + secondary electron (SE)) micrograph of the wave crest region showing formation of an intermetallic inclusion surrounded by a heat affected zone (HAZ) of the steel base material (a). Selected area diffraction patterns of the FeTi phase (b) and metastable  $\text{Fe}_{9.64}\text{Ti}_{0.36}$  phase (c) acquired via FIB sample preparation and following TEM analysis from the regions highlighted in (a).

Cracks only occur in brittle FeTi and metastable  $\text{Fe}_{9.64}\text{Ti}_{0.36}$  intermetallic phases (phase identification was conducted via TEM diffraction pattern analysis) and do not expand into the surrounding material. The grains on the steel-rich side on top of the intermetallic inclusion reveal a recovered and recrystallized morphology. Such grains morphology was often found in the base materials surrounding the intermetallic inclusions.

### 3.3. Nano-scale investigation of the interface region

Fig. 6a illustrates a typical portion of the interface region between the joined components using TEM bright field contrast and corresponding diffraction pattern (the regions from which the diffraction patterns were collected are highlighted: SAD, selected area diffraction; NBD, nano-beam diffraction). Examination of the interface microstructure at the nanoscopic scale reveals two components with different morphologies. The dominant one, adjacent to steel, consists of strongly deformed nano-size crystallites and therefore shows absence of typical crystalline contrast during tilting in the TEM. In contrast, the intermetallic component adjacent to Ti is much coarser and consists of well define grains (up to 30 nm in diameter). The overall thickness of the intermetallic layer varies in range between 100 and 300 nm while its morphology does not change significantly. The chemical composition of the dominant, close to amorphous phase varies from 80 to 56 at.% Ti and 20 to 44 at.% Fe, respectively, as determined by EDX in TEM. However, the electron diffraction patterns acquired from this region so far do not allow for unambiguous phase identification. An example of nano-beam (probe size of 5 nm diameter) electron diffraction (NBD) pattern collected from the dominant reaction product of the interface is shown in Fig. 6b. The pattern appears very unsharp which indicates large distortions of the crystallographic unit cell.

### 3.4. Fracture analysis

Fracture surfaces obtained from tensile tests were analyzed with respect to the microstructural origin of failure and fracture mechanism. Investigated joints failed at an ultimate tensile strength of 220 MPa normal to the bonding interface which is ~46% below the yield strength of the low carbon steel substrate plate. The SEM images reveal features that are characteristic of brittle fracture, Fig. 7. EDX analysis of the fracture surfaces (Table 2) shows the presence of the two previously reported intermetallic phases, namely, FeTi and metastable  $\text{Fe}_{9.64}\text{Ti}_{0.36}$ . Both intermetallic compounds and the Ti rich side show typical cleavage fracture, while the steel reveals a transgranular fracture mode.

The fine equiaxed grains surrounding the intermetallic inclusion on the steel-rich side were already shown in Fig. 5.

Since the fractured surface contains both base materials and the two main reaction products (FeTi,  $\text{Fe}_{9.64}\text{Ti}_{0.36}$ ) it is from the current data not yet clear how exactly the cracks form and propagate under tensile loads. Of particular relevance in that context are the micro-cracks that occur within the intermetallic phases (arrows in Fig. 7).

### 3.5. Bending test

The bending tests were performed to evaluate the influence of the micro-cracks on the integrity of the joints and the locations of the cracks at an early stage. The tested specimens were deformed up to 90° bending angle. No separation of the components was observed. Fig. 8 shows SEM micrographs of the specimen before (a) and after (b) a three-point bending test. Fig. 8b reveals that the cracks which were originally localized within the intermetallic region (Fig. 8a) start to expand into the steel microstructure. Fig. 8a reveals that micro-cracks occur not only within the intermetallic phases but also at the interfaces (arrows pointing down) of the joint.

**Table 2**

Chemical composition of the selected points on the fractured surface shown in Fig. 7.

Area	Ti (at.%)	Fe (at.%)
A	53	47
B	23	77
C	–	100

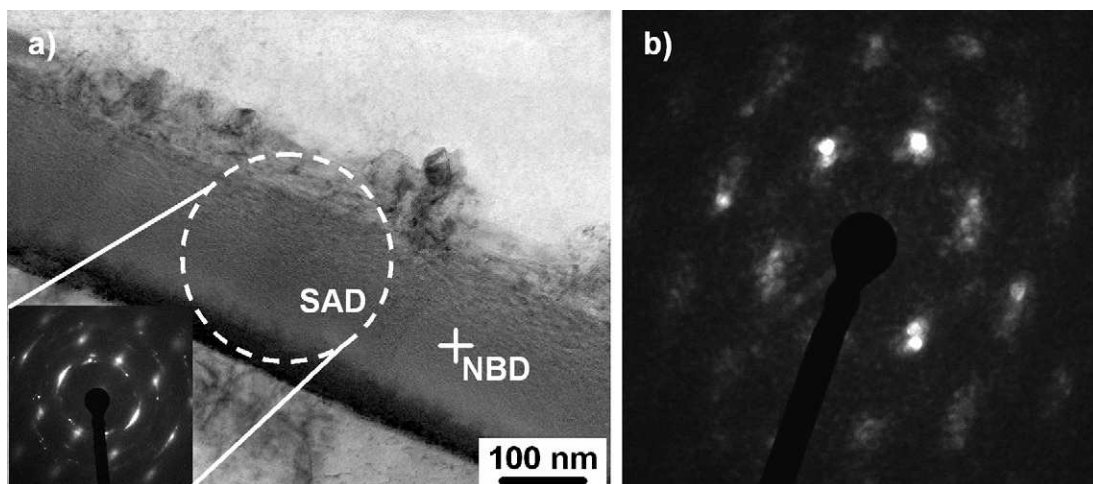


**Fig. 6.** TEM micrograph showing the formation of nano-grained intermetallic phases at the interface region and corresponding selected area electron diffraction (SAD) pattern (a) and a nano-beam electron diffraction (NBD) pattern acquired from the middle of the reaction layer (probe size 5 nm diameter) (b).

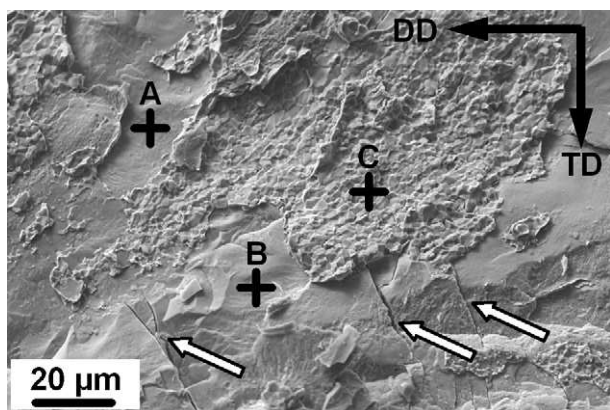


**Fig. 7.** Fracture surface micrograph (SE) showing cleavage fracture and micro-cracks propagating within the intermetallic phase (arrows). EDX analyses (see Table 2) reveal that the fine grained region corresponds to the steel, while the remaining regions correspond to intermetallic phases (with cracks) and pure Ti.

However, the analysis also shows that during mechanical loading these pre-existing interface cracks do not extend as significantly as the cracks in the FeTi phase (arrow pointing up) which extend into the steel substrate upon loading, Fig. 8b.

#### 4. Discussion

The microstructure of the interface region of the Ti to steel explosive joint is characterized by four successive, hierarchical microstructure levels, Fig. 9.

Each hierarchical scale reveals characteristic features. The interplay of different phases and defect scales under load is important to understand the mechanical behavior of the bonding and for optimizing the explosive joining parameters. As the final microstructure is a consequence of several metallurgical processes occurring during joining the discussion follows the kinetic sequence leading to the various hierarchical units.

After the ignition of the explosion the Ti cladding plate accelerates towards the base steel plate. A propagating jet forms between the two plates. It removes the oxide layers from the two materials. Ideally, at impact the oxide-free surfaces then interact at atomic range providing optimal metallurgical bonding. An optimal design of the collision of both materials is essential for the microstructure–property relationships of the compound as it determines the level of plastic deformation induced and possible melting

of the base materials. The amount of accumulated strain and the temperature rise depend on the impact energy. When high explosive velocities and high stand-off distances are applied the microstructure in the interface region reveals enormous deformation gradients and multiple new phases. Our observations agree with previous results which document that the flyer plate (Ti in this case) always undergoes higher deformation than the base material (steel in this case) [20]. Strongly deformed zones surrounding the interface region (Figs. 3 and 9) have strong influence on the physical, mechanical, and thermal properties of the compound. On the

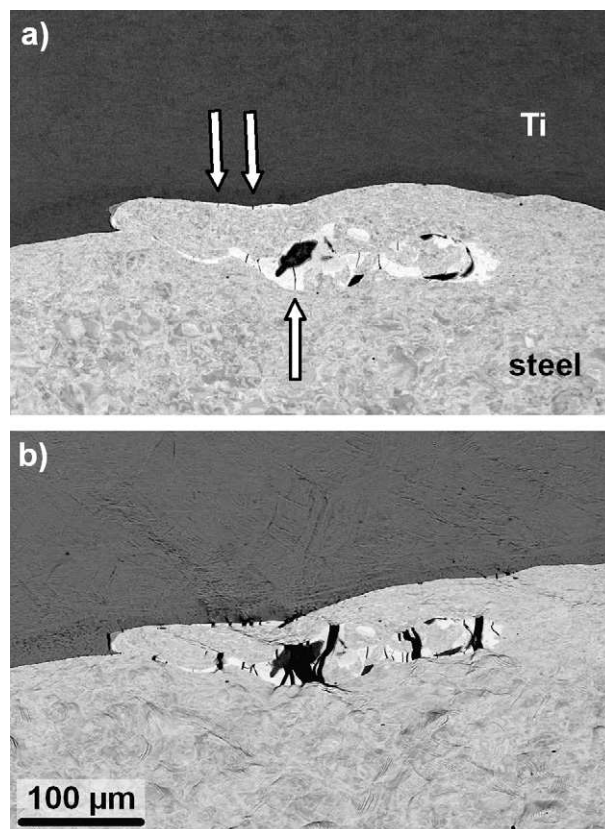


**Fig. 8.** SEM (BSE) micrographs of the specimen before (a) and after (b) three-point bending test. The arrows indicate the presence of microcracks within the FeTi intermetallic phase (arrow pointing upward) and at the interface (arrows pointing down).

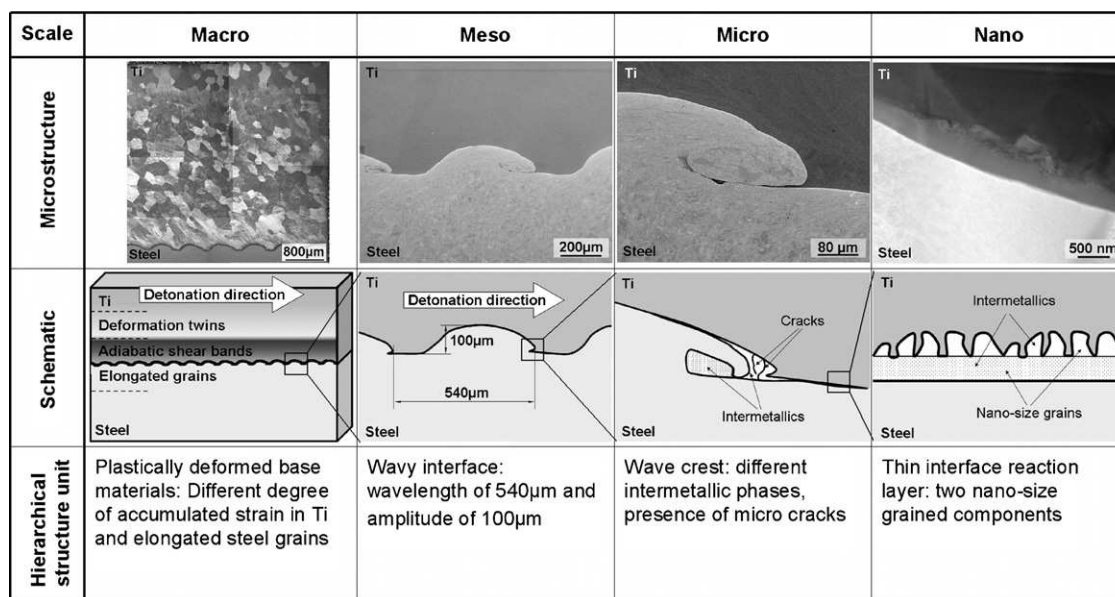


Fig. 9. Hierarchical structure levels at the interface region of the dissimilar explosive cladding joints of Ti to steel.

one hand the strong deformation leads to an overall high strength of the interface zone and to a highly graded microstructure as the strain level decays as a function of the spacing from the joining interface. On the other hand too intense deformation may lead to high dissipative and near-adiabatic heating and – as a consequence – to recovery, recrystallization, or even larger melting zones.

The collision impact angle which is determined by the explosive force, the jet, and the stand-off distance, is responsible for the formation of the second hierarchical level, Figs. 3, 4a and 9, namely, the wavy interface. The hydrodynamical aspects controlling the wave formation during explosive welding were addressed earlier [21–26]. According to these results, the wavy interface is caused by an oscillation in the jet flow, which depends on the velocity of the collision. To ensure deformation of the metal surfaces by the jet, the pressure generated immediately ahead of the collision point must be of sufficient magnitude to exceed the dynamic elastic limit of the material. The amplitude and wavelength of the interface waves are controlled by external parameters, i.e. the amount of explosive and the stand-off distance which together determine the collision angle. The wavelength and amplitude in turn influence the jet energy that can get trapped between the joined plates. The trapping of extremely high kinetic jet energy leads to local melting of the component with the lower melting point. This means that local melting can origin from both, trapped jet energy and dissipative deformation heating. Previous papers suggest [21–26] that the latter mechanism is of lower relevance compared to direct melting through the jet energy captured in narrow interface waves. A good quality explosion weld is obtained only when an optimum jet is formed. In a case that the jet becomes too large in magnitude, the weld interface will contain large amount of molten material.

The 3rd hierarchical interface level (micrometer scale) reveals molten material that solidified in the form of intermetallic inclusions, Figs. 4b, 5 and 9. When a melt zone is produced in the wave peak region, the displacement boundary conditions imposed by the solid material around it lead to a circular movement and intense stirring of the melt leading to strong intermixing of Ti and steel.

This mechanism leads to a microstructure where the intermetallic inclusions form at the wave crests rather than at the wave peaks. It is obvious that these melt droplets are rapidly quenched by the surrounding material. However, liquid state diffusion and high local pressure in these zones drives chemical reactions

which may lead to complex non-equilibrium new phases. Fig. 5 shows that the inclusion reveals a swirl-like contrast indicating strong chemical gradients and consequently different intermixing and possibly also different phases formed during solidification. These intermetallic inclusions do not follow the Ti–Fe equilibrium phase diagram, i.e. phase identification must be conducted using electron diffraction rather than only chemical compositions analysis.

Another microstructural feature at this hierarchical level are multiple recrystallized grains surrounding the intermetallic inclusions, Figs. 5 and 9. They appear as a result of the heat transfer between the melt and the heavily deformed base material. As the heat-affected zones observed around the inclusions are very small in comparison to the work hardened base materials, their softening contribution to the overall mechanical bulk properties of the material may be small. In contrast, the amount, dispersion, and ductility of the intermetallic phases along the joining interface have a large effect on the properties of the compound, specifically on the toughness and fracture type.

The next (4th) hierarchical level is characterized by a thin reaction layer consisting on nano-sized intermetallics, Figs. 6 and 9. The collision pressure and the temperature rise associated with the dissipation of the kinetic energy are supposedly high enough to promote direct inter-atomic bonding between the two metals (Ti, Fe). Besides such immediate bonds the two abutting heavily deformed materials have increased diffusion rates owing to their high defect density [27]. This effect results in an increased reaction rate which leads to the formation of thin layers of intermetallic compounds along the interface. The structure of this reaction layer remains unclear obviously due to strong distortions of the crystallographic unit cell (Fig. 6b) even within tiny volume (nano-beam electron diffraction from 5 nm diameter region) and large chemical gradients (concentration of Ti changes from 80 to 56 at.% within distance of 200 nm). The extreme thermodynamic conditions associated with explosion joining, hence, cause formation of new, highly metastable crystal structures which so far were not reported in the crystallographic data bases. The very thin interface reaction layer ( $\approx 100$ – $300$  nm) is the main, dominating component along the interface length that ensures good macroscopic bonding between the joined components. Its formation is very complex and involves both mechanical alloying and solid-state reaction

processes occurring at very high pressure, high local heating and subsequent rapid cooling.

The direct correlation between microstructure and properties of Ti to steel explosive clad joints is challenging owing to the structural complexity of the bonding zone as outlined above. The discussion of the interface zone in terms of its pronounced hierarchical microstructure helps to understand the specific influence of some of the features on the strength of the joint in a more systematic way.

The analysis of the fracture surfaces after tensile testing shows the presence of the original materials and their reaction products. Failure initiation starts with the cracks inside of the intermetallic phase discussed above (Figs. 5 and 7).

When subjecting the joined components to a bending load the small cracks that pre-existed inside the intermetallic phase areas did not extend further as observed at the nanoscopic scale (Fig. 8).

However, when probing the hard intermetallic inclusions and the recrystallized grains that surround them at the microscopic scale we observed the formation of new cracks inside some of these brittle FeTi intermetallic zones. However, as a rule these did not expand from the cracks that were formed during the cladding process.

We explain these new cracks by the following mechanism: during cooling after cladding stresses associated with the phase transformation, impact-induced lattice defects, and differences in thermal expansion of the intermetallic inclusions and the steel lead to local stress peaks that will eventually cause cracking. The mismatch in the linear coefficients of thermal expansion (CTE) of low carbon steel ( $\sim 14.2 \mu\text{m}/(\text{m K}^{-1})$ ) and FeTi ( $\sim 13.7 \mu\text{m}/(\text{m K}^{-1})$ ) [28] is not significant, though. Hence, it is not likely that the difference in thermal expansion alone causes the cracks in the brittle FeTi inclusions during cooling. During bending some newly generated cracks appear and grow together with these pre-existing ones. This observation suggests that the forming limits and the high intrinsic Peierls barriers lead to insufficient plastic compliance of the intermetallic inclusions relative to the surrounding matrix.

Upon bending the strain is mainly accumulated by the recrystallized grains of the steel base material that surround the intermetallic zones. The presence of a heat affected zone around the brittle intermetallic components compensates local strain peaks and does not allow for easy crack propagation, i.e. the softened matrix is assumed to be damage tolerant as it promotes crack blunting and plastic energy dissipation before the crack tips. The contribution of the mesoscopic scale to the overall mechanical properties within this hierarchical microstructure setting is difficult to estimate: generally the heavily work hardened interface areas that pertain to the former bulk materials significantly improve the strength of the joint. Also, all transformations and local deformation mechanisms observed (except for the formation of the intermetallic inclusions) are volume-conserving. On the other hand the neighbored hardening and recrystallization events obviously insert stress and strain gradients that might lead to further damage at the transition zones between such soft and hard areas inside the material when exposed to mechanical loads. However, altogether this effect does not seem to promote further damage initiation or further failure percolation under bending loads. Our empirical data clearly reveal that the entire joints show excellent

integrity at each hierarchical level even up to 90° elastic–plastic bending.

## 5. Summary

The interface region of explosively clad metallic joints, here demonstrated using the system Ti–steel, reveals a complex microstructure which consists of four successive hierarchical levels: the mesoscopic scale shows a wavy interface (wavelength  $\approx 0.5$  mm) which is due to the plastic shear waves that expand during the explosion. At the microscopic scale we observed intermetallic FeTi and  $\text{Fe}_{9.64}\text{Ti}_{0.36}$  inclusions ( $\approx 100$ – $200 \mu\text{m}$ ) that result from partial melting. These inclusions often contained micro-cracks that did not expand into the bulk materials. At the smallest hierarchy level we found a reaction layer of about 100–300 nm thickness consisting of nanocrystals. The type, brittleness, and the abutting microstructure of the intermetallic zones play the dominant role for the overall mechanical performance of the compounds when exposed to tensile and bending loads.

## Acknowledgements

The authors thank for the financial support of International Max Planck Research School for Surface and Interface Engineering in Advanced Materials (IMPRS-SurMat) and DMC Dynaplat GmbH&Co.KG for providing good quality clad joints.

## References

- [1] S.A.A. Akbari Mousavi, P.F. Sartangi, *Mater. Des.* 30 (2009) 459–468.
- [2] T.Z. Blazinsky, *Explosive Forming, Welding and Compaction*, Elsevier Science, New York, 1983.
- [3] B. Crossland, *Explosive Welding of Metals and its Application*, Clarendon Press, New York, 1982.
- [4] S.A.A. Akbari Mousavi, P.F. Sartangi, *Mater. Sci. Eng. A* 494 (2008) 329–336.
- [5] P. Manikandan, K. Hokamoto, A.A. Deribas, K. Raghukandan, R. Tomoshige, *Mater. Trans.* 47 (2006) 2049–2055.
- [6] K. Hokamoto, Y. Ujimoto, M. Fujita, *Mater. Sci. Forum* 426–432 (2003) 4039–4044.
- [7] S.R. Reid, *Int. J. Mech. Sci.* 16 (1974) 399–413.
- [8] S.H. Carpenter, R.H. Wittman, *Ann. Rev. Mater. Sci.* 5 (1975) 177–199.
- [9] V.G. Petushkov, *Combust. Explos. Shock* 36 (2000) 771–776.
- [10] G.R. Cowan, O.R. Bergmann, A.H. Holtzman, *Mater. Trans.* 2 (1971) 3145–3155.
- [11] N. Kahraman, B. Guence, F. Findik, *J. Mater. Proc. Technol.* 171 (2005) 241–249.
- [12] J.H. Han, J.P. Ahn, M.C. Shin, *J. Mater. Sci.* 38 (2003) 13–18.
- [13] A. Abe, *J. Mater. Process. Technol.* 85 (1999) 162–165.
- [14] U.K. Mudali, B.M.A. Rao, K. Shanmugam, R. Natarajan, B. Raj, *J. Nucl. Mater.* 321 (2003) 40–48.
- [15] R. Kaçar, M. Acarer, *J. Mater. Process. Technol.* 152 (2004) 91–96.
- [16] F. Grignon, D. Benson, K.S. Vecchio, M.A. Meyers, *Int. J. Impact. Eng.* 30 (2004) 1333–1351.
- [17] J. Dor-Ram, B.Z. Weiss, Y. Komen, *Acta. Metall.* 27 (1979) 1417–1429.
- [18] Y. Li, H. Hashimoto, E. Sukekai, Y.M. Zhang, *J. Electron. Microsc.* 49 (2000) 5–16.
- [19] L.D. Anikina, G.I. Berdichevskii, V.I. Mall, T.M. Sobolenko, *Combust. Explos. Shock* 6 (1970) 120–122.
- [20] M. Nishida, A. Chiba, K. Imamura, H. Minato, J. Shudo, *Metall. Mater. Trans. A* 24 (1993) 735–742.
- [21] A.S. Bahrani, T.J. Black, B. Crossland, *Proc. R. Soc. A* 296 (1967) 123–136.
- [22] G.R. Abrahamson, *J. Appl. Mech.* 83 (1961) 519–528.
- [23] W.E. Clausen, A.W. Leissa, AFML-TR-67-15, AD-656431, 1967.
- [24] A. Ben-Artzy, A. Stern, N. Frage, V. Shribman, O. Sadot, *Int. J. Impact. Eng.* 37 (2010) 397–404.
- [25] A. Szecket, *Mater. Sci. Eng.* 57 (1983) 149–154.
- [26] J.L. Robinson, *J. Fluid Mech.* 63 (1974) 723–752.
- [27] A. Oberg, N. Martensson, J.A. Schweitz, *Metall. Trans. A* 16 (1985) 841–852.
- [28] Y. Terada, *Platinum Met. Rev.* 52 (2008) 208–214.